

Review article

Natural variability of shoreline position: Observations at three pocket beaches

I. Turki ^{*}, R. Medina ¹, M. Gonzalez ¹, G. Coco ¹

Environmental Hydraulics Institute "IH Cantabria", University of Cantabria, c/Isabel Torres 15, 39011 Santander, Spain

ARTICLE INFO

Article history:

Received 6 February 2012

Received in revised form 27 September 2012

Accepted 14 October 2012

Available online 6 November 2012

Communicated by J.T. Wells

Keywords:

shoreline variability

empirical orthogonal functions

pocket beaches

shoreline rotation

ABSTRACT

We investigated the variability of shoreline position of three adjacent pocket beaches at Barcelona city (NW Mediterranean) over a period of two years. Daily measurements of shoreline position were extracted from high-resolution video images and used to determine shoreline variability. Using empirical orthogonal function analysis we determine two dominant modes of shoreline variability. For all beaches analysed the mode that explains most of the variability (around 70%) describes the beach plan-form rotation which primarily occurs at the seasonal scale. The cross-shore translation of the beach profile, is described by the 2nd mode which explains around 30%. Both types of shoreline movement have been related to the previous nearshore conditions. This relationship was explored standardizing the translation/rotation of the shoreline and comparing it with time-averages of the cross-shore energy flux (EF_{csh}) and the energy flux direction (EF_D). Averages over 7 to 12 days of EF_{csh} were significantly correlated to the translation movement. Plan-form rotation was well described by 28 to 40 day-averaging of EF_D . Comparing results from the three beaches we determined that the time required to average the previous wave conditions depends on the beach characteristics (beach length and sediment grain size) in such a way that the greater the length of the beach and its sediment grain size, the slower its response.

© 2012 Elsevier B.V. All rights reserved.

1. Introduction

Understanding and predicting shoreline variability remains one of the core problems in nearshore science and coastal engineering. The different timescales and (often nonlinear) processes involved with shoreline variability make this problem an unsolved challenge with implications that are relevant to coastal managers (e.g., the development of setbacks and hazard zones) and the general public. Variability in shoreline position is a reliable proxy to describe overall beach change (Smith and Bryan, 2007) and has often been used to study short (order of days to seasons) and long (order of years and longer) time scales. Shoreline variability can in fact be used to assess the effect of individual storms, seasonal changes in wave forcing and even processes related to climatic patterns. An example of the long time-scale is given by Harley et al. (2010) who used a multi-decadal beach survey dataset at a coastal embayment in Sydney, Australia, to identify erosion/accretion cycles coinciding with variations in the El Niño/Southern Oscillation. At the shorter temporal scale, mean variations of shoreline position have been correlated with seasonal changes in wave climate (e.g., Winant et al., 1975; Aubrey, 1979).

Datasets of shoreline positions can also be used to develop and test predictive models. For example, Davidson et al. (2010) developed a simple numerical model that addresses shoreline variations and that depends on the wave-averaged conditions over the previous days. Using data from the Gold Coast (Australia), the model was then calibrated at the storm and seasonal time-scale using averages of the previous wave climate (Davidson et al., 2011). Results indicated that averaging the wave climate beyond 2 days deteriorates model performance while averaging beyond 40 days (which implies smoothing out the effect of individual storms) results in a strong decay of the model performance. These findings depend primarily on the local wave climate (e.g., storm frequency) and it is likely that they will vary on beaches characterized by different geomorphic setting.

To develop this type of models, high resolution (in time and space) datasets are needed and different remote-sensing techniques such as radar (e.g., Frasier et al., 1995), LIDAR (e.g., Robertson et al., 2004), and video (e.g., Holland et al., 1997) have been developed. Data from video systems probably offers the best compromise in terms of costs, and spatial and temporal resolution. Aside from shoreline detection, video systems have been used to study various coastal characteristics like, for example, intertidal beach profile (Aarninkhof et al., 2000), underwater bathymetry (e.g., Stockdon and Holman, 2000), sandbar variability (e.g., Holman and Lippmann, 1987), runup and rip channel dynamics (van Enckevort et al., 2004; Guedes et al., 2011). Overall, video-systems have become an extremely popular tool for coastal management (Davidson et al., 2007). Amongst the data available through video, shoreline position is critical to coastal zone management because

^{*} Corresponding author at: UMR CNRS 6143 Continental and Coastal Morphodynamics 'M2C' University of Rouen, 76821 Mont-Saint-Aignan Cedex, France. Tel.: +33 2 35 14 69 50, +33 6 52 90 02 52; fax: +33 2 35 14 70 22.

E-mail addresses: turkimen81@gmail.com (I. Turki), medinar@unican.es (R. Medina), gonzalere@unican.es (M. Gonzalez), cocog@unican.es (G. Coco).

¹ Now at UMR CNRS 6143 Continental and Coastal Morphodynamics 'M2C' University of Rouen, 76821 Mont-Saint-Aignan Cedex, France.

temporal variability in shoreline position quantifies beach plan-form variations (Farris and List, 2007) and is a good indicator of erosion/accretion patterns.

Beach variability can be studied using statistical methods such as empirical orthogonal function (EOF) analysis. Early studies applying EOFs to coastal data are described in Miller and Dean (2007a). Miller and Dean (2007a, 2007b) also used EOFs to investigate patterns of alongshore variability on different beaches worldwide. Findings show that, when present, cross-shore structures (e.g., engineering structures or natural headlands) affect and in some cases even dominate shoreline behaviour. At the only site where no shore-perpendicular structure was present (Gold Coast, Australia), EOF allowed identification of rhythmic alongshore morphological patterns at a variety of spatial scales. Miller and Dean (2007b) found that the strongest correlations between the first EOF mode and nearshore parameters were the ones involving a monthly average of the wave characteristics. Correlations between other modes and nearshore parameters depended on the specific beach characteristics and local wave climate. Fairely et al. (2009) have used EOFs to decompose a video derived shoreline dataset at Sea Palling into the dominant modes of shoreline change behind detached breakwaters affected by the same wave climate but characterized by different design schemes. They found that the first and second EOF modes were related to the cross-shore and alongshore migration of the salients/tombolos. They also showed that modes can be correlated to a combination of tidal range and wave characteristics.

Pocket beaches are more common than generally thought and represent about 50% of the world's coastline (Short and Masselink, 1999). These beaches are typically protected by structures or geological constraints so that sediment bypasses tend to occur subaqueously (Short et al., 2000). They are also characterized by the formation of rips (Holman et al., 2006) and by beach rotation, i.e. lateral movement of sand along the beach in response to a modification in the incident wave direction (Short and Masselink, 1999). Beach rotation has been observed on many coastlines including Brazil (Klein et al., 2002; Martins et al., 2010), Spain (Ojeda and Guillén, 2008), New Zealand (Bryan et al., 2009) and Australia (Short et al., 1995; Masselink and Pattiaratchi, 2001). Ranasinghe et al. (2004) established a link between the southern Oscillation Index (SOI), wave climate and beach rotation at the southern and central coastline of New South Wales, Australia. Ojeda and Guillén (2008) analysed the shoreline evolution of artificially embayed beaches of Barcelona during 2001–2004. They associated rotation events not only to storms but also to engineering operations (nourishment and sand relocation). Ruiz-De-Alegría-Arzaburu and Masselink (2010) explored fortnightly measurements of subaerial morphology from a steep macrotidal gravel beach on the south-west coast of the UK. They found that the stability of the beach and its rotation, at the annual time scale, depends on the relative contributions of the storm types. Harley et al. (2012) used thirty years of wave and beach survey data at Collaroy–Narrabeen beach in SE Australia to investigate the extent to which shoreline rotations within a coastal embayment are dominated by cross-shore and alongshore exchanges. Their analysis was also based on EOF and indicated that the first and second modes, explaining 60 and 24% of the total variance, can be related to beach translation and beach rotation, respectively. Also, beach rotation appeared to be responding to wave climate in a distinctly different way than beach translation.

Few studies have addressed seasonal to annual patterns in beach rotation and so far, to our knowledge, no study has related the details of beach plan-form rotation to the geomorphic characteristics of the beach.

In the case of the present research, video imaging techniques were used to measure the shoreline position (e.g., Aarminkhof et al., 2003; Osorio, 2006; Ojeda and Guillén, 2008). The focus is to achieve a better understanding of the shoreline variability and response to nearshore wave conditions in three artificially embayed beaches of Barcelona, in the NW Mediterranean coast.

Although over a different period than the one herein considered, two of these beaches have already been studied (Ojeda and Guillén, 2008; Ojeda et al., 2010, 2011) to assess how beach rotation can be the response to man-made engineering works or to individual storms. In particular, Ojeda et al. (2010, 2011) have used 4.3 years of video-images to analyse morphological changes (response of the shoreline and the submerged sandbars) as a result of storm events showing that both short-term cross-shore and inter-annual onshore bar migration can be related to wave height and water depth. During the period considered in this study, no anthropogenic activity was present.

The possibility of studying three neighbouring beaches subject to the identical wave climate provides an ideal setting to analyse the role of geomorphic beach characteristics on shoreline dynamics. In the following sections, beach variability is analysed using empirical orthogonal functions (EOFs) while response to wave climate is explored by studying how beach translation and rotation are related to the previous wave energy.

2. Study area: Barcelona city beaches (Spain)

The coast of Barcelona contains a series of artificially embayed beaches enclosed by perpendicular groins at the sides and a promenade at the back created in 1992. Barcelona's beaches are regularly nourished and often affected by human activities such as sand cleaning and sand redistribution after the storms. This study focuses on three pocket beaches along the city (Fig. 1a): Bogatell, Nova Icaria and Somorrostro. During the period analysed, 2005 to 2007, no defined human activities affecting the sediment budget or the large scale overall beach shape (beach nourishments and sand redistribution along the beach after storms) were carried out, so that the natural variability of the shoreline position could be analysed. Physical characteristics of Barcelona city beaches (length, orientation, average slope and sediment grain size) are shown in Table 1. Bogatell has the highest sediment grain size (0.75 mm) and length (600 m). Nova Icaria is characterized by the same sand material and a length of about 400 m. This length is the same as in Somorrostro where the mean grain size is 0.45 mm.

3. Methodology

3.1. Nearshore observations

Wave data were provided by the Spanish Port Authority (<http://www.puertos.es>).

Data was obtained from a directional wave buoy placed in front of Barcelona harbour (Fig. 1). The wave buoy provides hourly significant wave height (H_s), peak period (T_p) and mean direction (Dir) from 8-March-2004.

According to buoy measurements, the wave-height timeseries is characterized by storm events separated by periods of low energy activity. During the study period, the mean significant wave height (H_s) is 0.7 m and the average peak period (T_p) is 5.5 s. The dominance of these waves is illustrated on the left side of Fig. 2b, with approximately 50% of all waves coming from the easterly (90° from the north) to south-easterly (135° from the north) directional sectors. 35% of waves are between south-east (135° from the north) and the south (180° from the north). The main wave directions are from east-south-east to south-south-east. Energetic events take place mainly during winter like the storms recorded on 31-Dec-2005 and 26-Jan-2006 when wave height reached 2.4 and 3 m in deep water, respectively. The timeseries of swell waves H_s in deep water is displayed in Fig. 2a.

The dominance of these waves is illustrated on the left side of Fig. 2b, with approximately 50% of all waves coming from the easterly (90° from the north) to south-easterly (135° from the north) directional sectors. 35% of waves are between south-east (135° from the

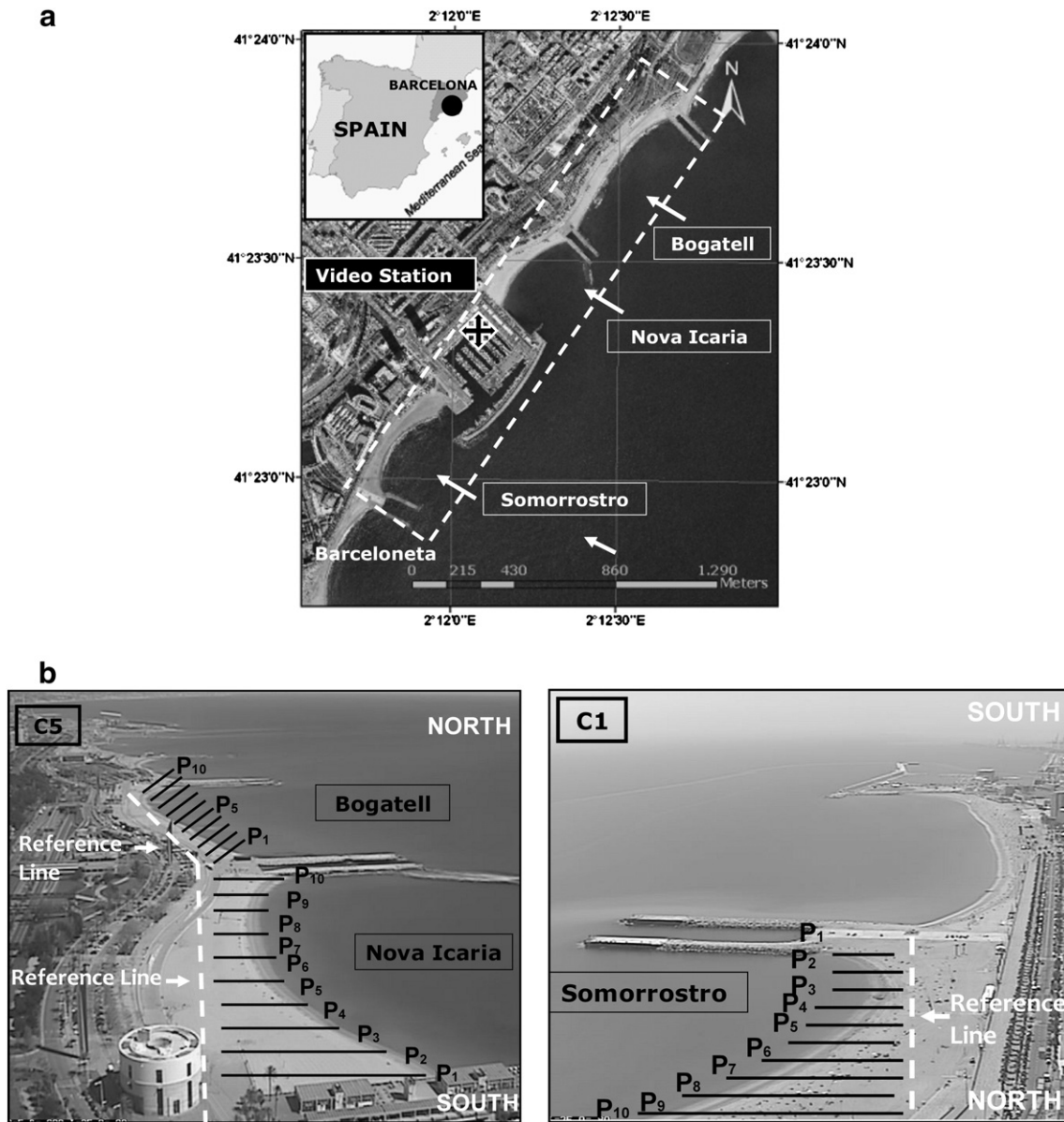


Fig. 1. (a) Study area; Barcelona City beaches. The location of the directional wave buoy placed in front of Barcelona harbour is defined by 2.20° E of longitude and 41.32° N of latitude. The harbour tide gauge is defined by of 2.16° E longitude and 41.34° N of latitude. (b) Oblique video images: Camera 1 (C₁) shows Somorrostro beach. Camera 5 (C₅) shows Bogatell and Nova Icaria beaches.

north) and the south (180° from the north). Fig. 2b indicates also a degree of seasonality in Barcelona wave climate. During winter months (middle side), wave distribution shows a dominance of waves coming from east to east–south–east. Between east–south–east and south, the

Table 1

Morphological characteristics of the three studied beaches: Bogatell, Nova Icaria and Somorrostro. Beach orientation is the mean value measured from video images with respect to the North; beach slope is the mean value obtained from 0 to 5 m water depth using a bathymetric survey carried out in March 2008; the sediment grain size is provided by samples collected near the swash zone.

Beach	Length (m)	Orientation (degrees)	Slope	D ₅₀ (mm)
Bogatell	600	40	0.032	0.75
Nova Icaria	400	42	0.045	0.75
Somorrostro	400	38	0.035	0.45

influence of waves is less than 40%. However, it is more than 60% during summer months (right side).

The coastal area of Barcelona, as most Mediterranean beaches, is microtidal. The astronomical tide is semi-diurnal with a mean range of 0.2 m. The total mean sea level is relative to Barcelona harbour. Storm surge can add 0.4 m to the astronomically-predicted tide level. Tidal data is obtained from a gauge, REDMAR, located within the Barcelona harbour. The gauge extracts the sea level (astronomical tide level and surge tide level data) every 5 min. This information was critical to select video images characterized, approximately, by the same sea level (see Section 3.2 in the next).

Offshore wave conditions obtained from a buoy were transformed into conditions at breaking using the numerical model SP-Oluca which is part of the Coastal Management System (SMC), a system developed by the Environmental Hydraulics Institute IH Cantabria (University of Cantabria). SP-Oluca solves the parabolic approximation of the Mild Slope equation and simulates the random sea over irregular bottom

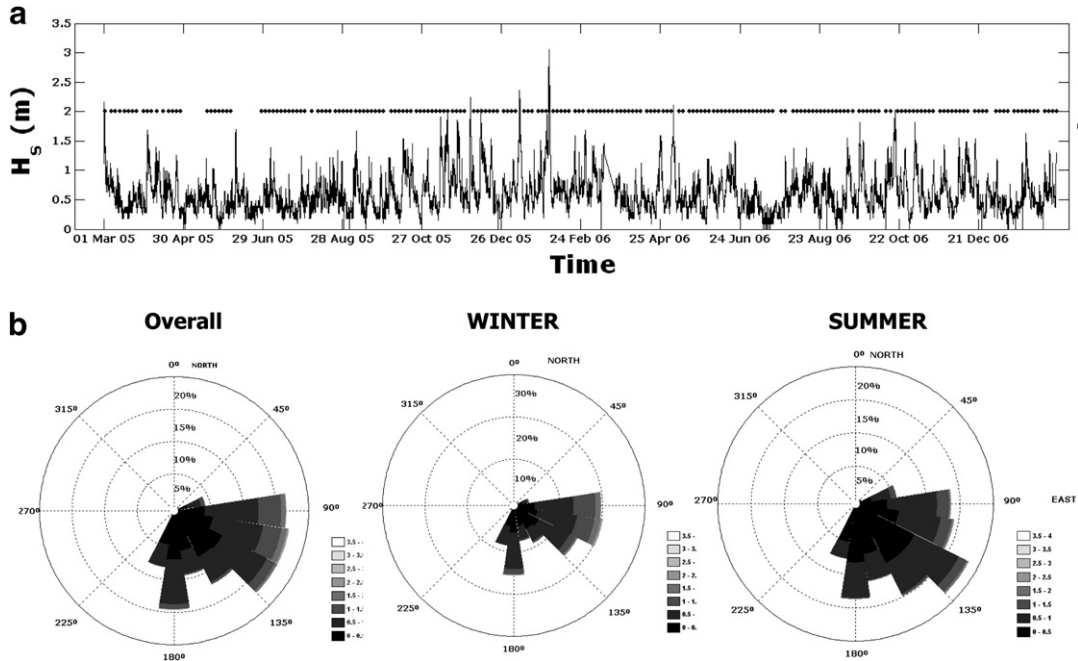


Fig. 2. (a) Timeseries of the significant wave height in deep water; the black points indicate dates when the shoreline could be extracted from video images. (b) Wave roses based on hourly data from Barcelona buoy for all months, winter months (December, January and February) and summer months (June, July, and August).

bathymetry (Gonzalez and Medina, 2007). Modelled waves (H_b, Dir_b) determined at the breaking zone ($H = \gamma \cdot h$) were used to calculate the energy flux EF .

$$EF = E \cdot Cg \tag{1}$$

where Cg is the group celerity and E is the total wave energy quantified using the root mean square wave height H_{rms} ($E = \frac{1}{8} \cdot \rho \cdot g \cdot H_{rms}^2$), k the wave number ($\frac{2\pi}{L}$), L the wave length ($\frac{gT^2}{2\pi}$), ρ the water density, g the gravity and h is the local water depth. H_{rms} and h were determined at the breaking zone.

EF_{csh} and EF_{lsh} are the cross-shore and the longshore components of the energy flux EF given as

$$EF_{csh} = EF \cdot \cos(\alpha) \tag{2}$$

$$EF_{lsh} = EF \cdot \sin(\alpha). \tag{3}$$

α is the angle between wave direction and the shoreline position.

Using EF_{csh} and EF_{lsh} , the energy flux direction EF_D can be determined as the following:

$$EF_D = \arctan\left(\frac{EF_{csh}}{EF_{lsh}}\right). \tag{4}$$

The timeseries of EF_{csh} and EF_D are displayed in Fig. 3a and b, respectively. Both EF_{csh} and EF_D were selected, after a series of empirical approximations, as the most appropriate parameters able to describe the shoreline movement. Following Gonzalez et al. (2010), the energy flux direction (EF_D) is selected as an appropriate forcing to describe the rotation of the beach platform. This quantity accounts not only

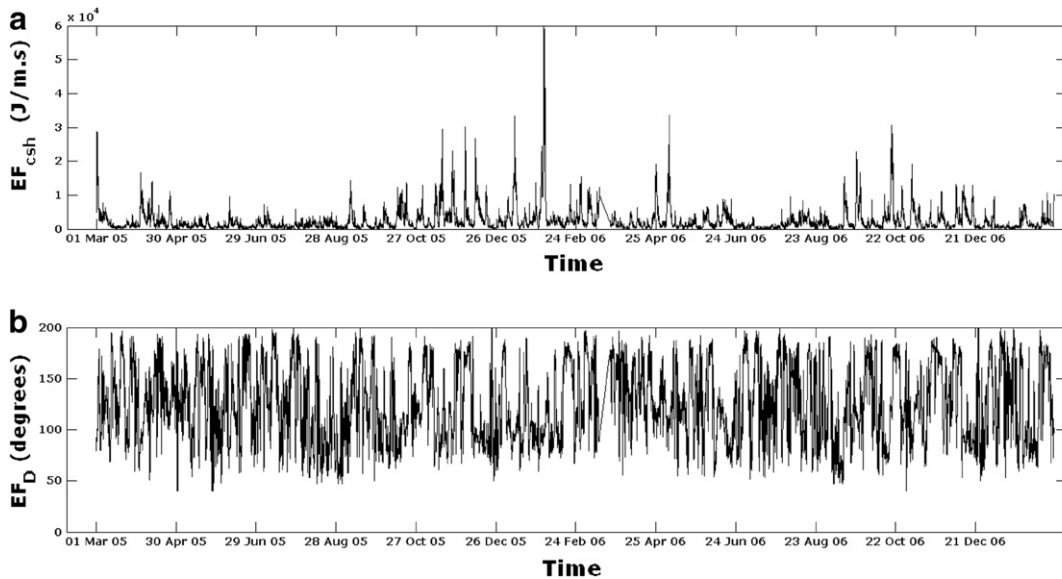


Fig. 3. The cross-shore energy flux EF_{csh} (a) and the energy flux direction EF_D (b) between March 2005 and March 2007 at Barcelona beaches.

for the wave direction but also for the amount of energy related to each specific wave direction.

3.2. Video imagery and shoreline detection

The shoreline position at each of the beaches was monitored using a video system (Holland and Stanley, 2007) located on a nearby building at a height of about 142 m (Fig. 1a). The monitoring station is composed of five cameras but only two of them, named C_1 and C_5 , are necessary to study the beaches considered in this work. Camera C_5 covers the Bogatell and Nova Icaria beaches while Somorrostro is captured by camera C_1 . With respect to Somorrostro beach, the northern part of the beach (approximately 50 m in length) has not been included in the analysis. This small area is strongly affected by a small jetty present on the beach which influences sediment transport patterns making shoreline dynamics different than the rest of the beach.

The images are collected every daylight hour for a ten-minute period. High-resolution video images were provided by the Coastal Ocean Observatory at Institute of Marine Sciences (CSIC) in Barcelona (Spain) where an image processor controls the capture, storage pre-processing and transfer of images. Images are available at <http://coo.icm.csic.es/content/video-monitoring>.

The shoreline mapping was detected manually as the wet/dry interface on the 10-minute averaged images. Shoreline positions extracted from oblique images were then rectified to real coordinates (Holland et al., 1997), a process that involves measurement of ground control points and the removal of radial lens distortion. The elevation of the wet/dry interface was based on the tide level within Barcelona harbour. Images were collected every hour (on the hour) and the closest image to the tidal level of +0.2 m was selected for analysis (this implicitly assumes that the mean water level is the same for the three beaches analysed). This implies that there might be a mist latch between the reference mean water level (+0.2 m) and the closest image. Nevertheless, if we consider the small tidal range of the beaches considered (0.4 m) we can safely assume that this error is small. The value of +0.2 m was chosen because the wet/dry interface was more easily detected during higher stages of the tide and because this value maximised the number of available images in relation to the spring–neap cycle.

Ten transects were extracted (P_1 to P_{10}) from each beach (Fig. 1b). The spacing between profiles was nearly 60 m in Bogatell and 40 m in Nova Icaria and Somorrostro. At each profile, shoreline positions detected from video images were compared to a bathymetric survey performed by the Iberport Consulting Company. In order to quantify the accuracy of the video-derived shorelines versus field measured shorelines, we calculated the root mean square error (RMSE) as

$$RMSE = \sqrt{\frac{\sum_{t=1}^n (Y_{\text{video},t} - Y_{\text{field},t})^2}{n}} \quad (5)$$

where Y_{video} and Y_{field} are the video-derived and DGPS-measured shoreline positions. n is the number of measurements. Results of RMSE, shown in Table 2, indicate that the error increases with the distance from the cameras. According to this analysis, the max RMSE of the shoreline derived from the video images is 1.2 m.

Shoreline extraction was based on the harbour tide gauge elevation (+0.2 m) being assigned to the video wet/dry interface which is also assigned an elevation based on the tide level within Barcelona harbour and represent approximately the open-coast water level.

Daily shoreline mapping was planned for each site with greater time resolution around storms. However, due to poor image clarity, shorelines were not always available and thus the temporal spacing between shorelines was not always constant. A total of 1050 shorelines having the same tide level (0.2 m) were extracted from the three beaches (350 shorelines for each one). Shoreline position was always measured with respect to a reference line (Fig. 1b).

Table 2

Root mean square errors (RMSE) of the video camera shorelines applying Eq. (5) at 9 different alongshore positions (profile) in Barcelona city beaches.

Profile	RMSE (m)
P_1 , Bogatell	1.2
P_5 , Bogatell	1.05
P_{10} , Bogatell	0.85
P_1 , Nova Icaria	0.65
P_5 , Nova Icaria	0.5
P_{10} , Nova Icaria	0.35
P_1 , Somorrostro	0.75
P_5 , Somorrostro	0.98
P_{10} , Somorrostro	1.17

3.3. Empirical orthogonal functions (EOFs)

Statistical methods have been used to identify patterns in morphological data and link them to physical processes (Larson et al., 2003). One of the most insightful techniques refers to the use of EOFs (Winant et al., 1975; Aubrey, 1979; Medina et al., 1991, 1994). This method aims to isolate the unrelated temporal and spatial modes and separate their dependence of the original dataset $Y(x,t)$ which can be written as a series of linear combinations of functions of time and space,

$$Y(x,t) = \sum_{k=1}^n C_k(t) \cdot E_k(x) \quad (6)$$

where $E_k(x)$ represents the spatial eigenfunctions, and $C_k(t)$ is the temporal eigenfunctions. The data $Y(x,t)$ is obtained by the summation from $k = 1$ to n where n is the lesser of the number of the temporal n_t and spatial n_x samples. Each combination $C_k(t) \cdot E_k(x)$ describes an orthogonal mode of change in the original dataset and its time variation. The first mode represents the most variance in the dataset.

Miller and Dean (2007a) decomposed the dataset into four modes of variability using EOF and described the first mode by the 'mean shoreline'; however in this paper, the original data set is demeaned (the mean value of shoreline change is removed) as we only focus on the shoreline variability. The von Storch and Hannstock (1984) algorithm was used to decompose the shoreline variability into different spatial and temporal eigenfunctions.

4. Shoreline movement

The total shoreline movement extracted from video camera was divided into two components: the first one designates the translation movement of the shoreline in the cross-shore direction; the second one represents the rotation movement and so the alongshore variation in beach plan-form. Both movements are conceptually summarized in Fig. 4. A series of n transversal profiles (P_1 to P_{10}) were considered along the beach and the shoreline position Ps was measured at each profile i and at a determined time t_j . Five quantities representing shoreline change can be defined:

1. The increment of the total shoreline movement $Ps_i(t_j)$ between two observations collected at the same location but different time, $Ps_i(t_j)$ and $Ps_i(t_{j-1})$, is

$$\Delta Ps_i(t_j) = Ps_i(t_j) - Ps_i(t_{j-1}). \quad (7)$$

The increment $Ps_i(t_j)$ includes both a translation $M_{\text{tr}}(t_j)$ and a rotation $M_{\text{rot}_i}(t_j)$ component (see Fig. 4a):

$$\Delta Ps_i(t_j) = M_{\text{tr}}(t_j) + M_{\text{rot}_i}(t_j). \quad (8)$$

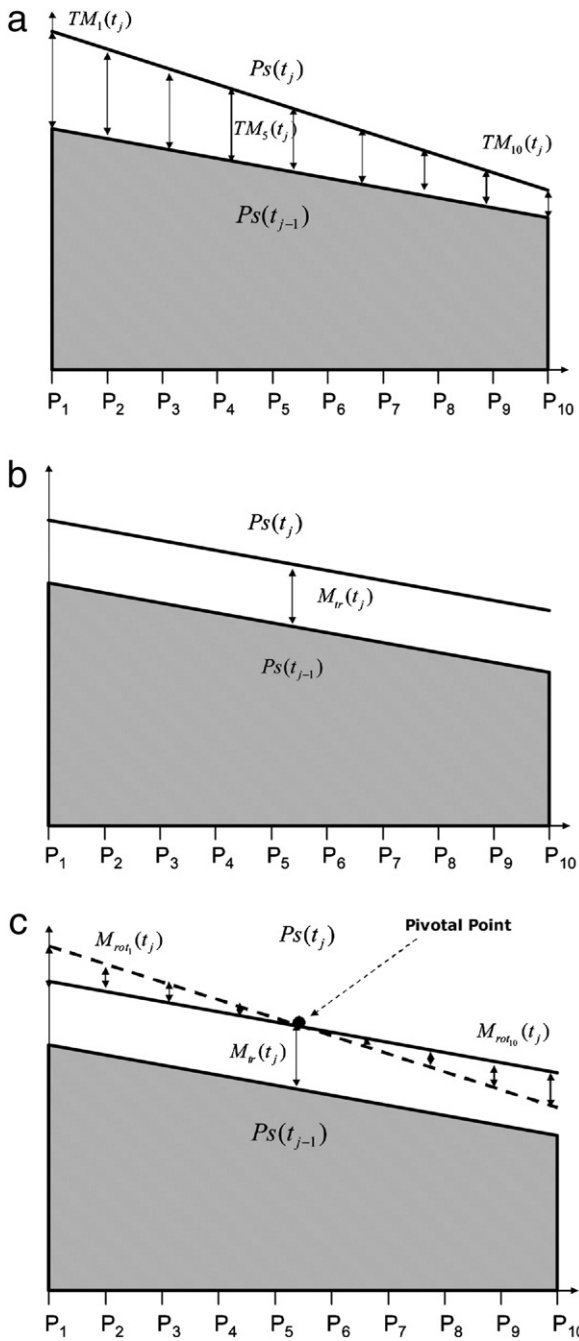


Fig. 4. Conceptual model used to quantify shoreline movements between Ps_{t_j} and $Ps_{t_{j-1}}$ at times t_j and t_{j-1} , respectively. (a) Total movement $Ps_i(t_j)$. (b) Movement of translation $M_{tr}(t_j)$. (c) Movement of rotation $M_{rot}(t_j)$ between two shoreline positions (solid and dashed-black line) around a pivotal point situated at the centre section of the beach.

2. The translation part is designated by $M_{tr}(t_j)$. It is assumed that this movement is, on average, the same along the beach

$$M_{tr}(t_j) = \frac{1}{n} \cdot \sum_{i=1}^n Ps_i(t_j) \quad (9)$$

where $n = 10$ (the number of shoreline positions), as seen in Fig. 4b.

3. The cumulative movement of translation $TM_{tr}(t_j)$ determined between the initial time t_0 (1-March-2005) and the time t_j can be calculated as

$$TM_{tr}(t_j) = \sum_{t_0}^{t_j} M_{tr}(t) \cdot \Delta t. \quad (10)$$

4. The increment in the rotation $M_{rot}(t_j)$ is calculated as (Fig. 4c)

$$M_{rot}(t_j) = \Delta Ps_i(t_j) - M_{tr}(t_j). \quad (11)$$

5. The cumulative movement of rotation $TM_{rot}(t_j)$ determined between the initial time t_0 (1-March-2005) and the time t_j can be calculated as

$$TM_{rot}(t_j) = \sum_{t_0}^{t_j} M_{rot}(t) \cdot \Delta t. \quad (12)$$

This conceptual model is a simplification of the shoreline movement which is, in reality, always a more complicated combination of translation and rotation without, for example, a clear pivotal point.

Translation and rotation changes were evaluated during the period March 2005–March 2007. Then, the relationship between the beach movement and the wave parameters was investigated. Both translation and rotation were associated to the preceding energy conditions.

Translational movement $TM_{tr}(t_j)$ was related to the cross-shore energy flux, averaged between 1 and k_{tr} days (k_{tr} is from 1 to 20), $EF_{csh}^{k_{tr}}(t_j)$.

$$EF_{csh}^{k_{tr}}(t_j) = \sum_{t=t_j}^{t=t_j-k_{tr}} EF_{csh}(t). \quad (13)$$

Rotational movement $TM_{rot}(t_j)$ was related to the energy flux direction, averaged between 1 and k_{rot} days (k_{rot} is from 1 to 55), $EF_D^{k_{rot}}(t_j)$.

$$EF_D^{k_{rot}}(t_j) = \arctan \left(\frac{\sum_{t=t_j}^{t=t_j-k_{rot}} EF(t) \cdot \sin(\theta_{wave}(t))}{\sum_{t=t_j}^{t=t_j-k_{rot}} EF(t) \cdot \cos(\theta_{wave}(t))} \right) \quad (14)$$

while θ_{wave} is the wave direction from the north reference.

Typically, wave measurements are available on an hourly basis while the frequency of the shoreline measurements ranged from daily to weekly. In order to compare the two timeseries using the correlation coefficient, both data sets must be sampled with the same time intervals. In this study we have reduced both datasets to the daily timescale. This implied averaging wave characteristics over 24 h while the timeseries of shoreline position had to be linearly interpolated when data was missing because of camera malfunctioning or because of weather conditions (the longest period with missing video data was three days).

5. Results

5.1. Shoreline variability

The original dataset for all transects (from P_1 to P_{10}) and beaches is presented in Fig. 5a where changes in the shoreline position show a succession of advances (red colour) and retreats (blue colour) during summer and winter times, respectively. These changes are not necessarily constant along the beach and are more pronounced at the northern side of the beaches under study. Large shoreline retreats are observed under high energy conditions, such as those occurring between October and November 2005, and sometimes also under smaller storms that follow periods of accretion (such as August 2005).

Then, EOFs were applied to the shoreline data. The first two eigenfunctions explain the majority of the shoreline change at the three beaches and overall typically account for about 98% of the total variability. For all beaches, the primary eigenfunction accounts between 70% and 80% of the total variability, while the second one between 18% and 27%. Results are summarized in Table 3.

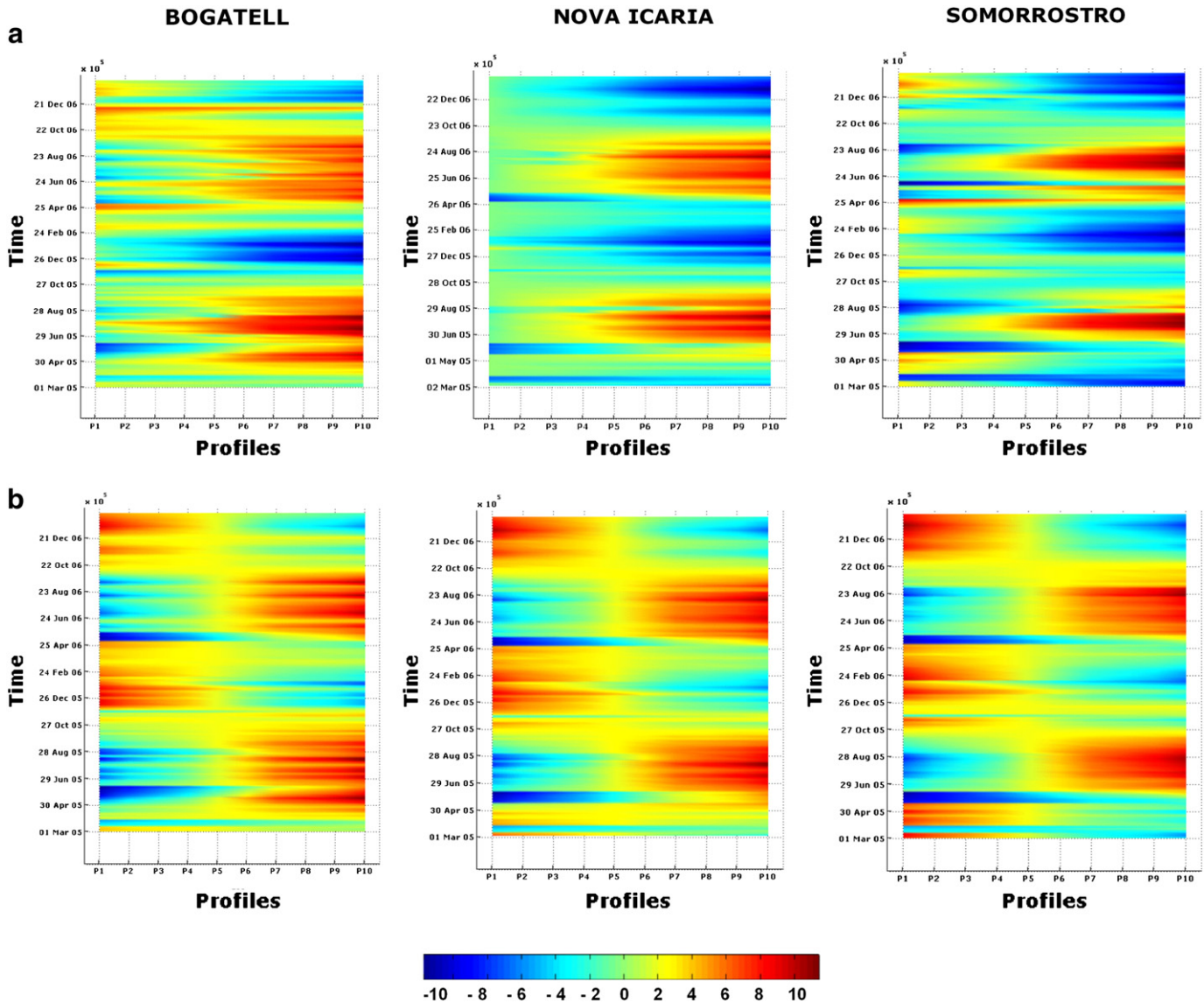


Fig. 5. (a) Shoreline position for all transects considered analyzed over the period of study. (b) Beach rotation evaluated using the conceptual model (Eq. 12).

The temporal variability given by $C_1(t)$ at the three beaches is shown in Fig. 6a. The dominant trend of this component consists of low frequency oscillations with a period of 1 year approximately. This temporal variability is evidenced by positive variations in summer (May–September) and negative ones in winter (October–April) which indicates the seasonal change of the shoreline position. Analysis of the temporal component shows a time-lag between the three beaches. $C_1(t)$ shows that the onset of change between summer and winter 2005 was faster at Somorrostro (dashed line) than at Nova Icaria (dotted line). In Bogatell, the response was the slowest (solid line).

The spatial eigenfunction $E_1(x)$, displayed in Fig. 6c, changes between negative and positive signs. This component stresses the main changes occurring over the beach plan-form with negative signs (erosion) at the southern side (from P_1 to P_5) and positive signs (accretion) at the northern side (from P_5 to P_{10}).

The first mode of the total shoreline variability, determined by the combined eigenfunction $E_1(x) \cdot C_1(t)$, is presented in Fig. 7. The plot shows that the shoreline position oscillates between -8 m and 8 m at all beaches. Positive and negative signs explain the accretion and erosion which mainly occur at the seasonal time scale. During winter periods, beach changes are negative at the northern side (P_{10}) and positive at the southern one (P_1). Overall, the beach retreats in the

north and advances in the south during high wave energy conditions. An opposite scenario can be observed in summer where the wave action is relatively moderate.

In essence, the first mode of shoreline change can be assigned to the plan-form rotation which occurs seasonally. The rotation is generally produced around a pivotal point so that the beach retreats at one end and advances at the other. In Bogatell, the pivotal point is located approximately on the central section of the beach (P_5) and a few metres away from the central section at the northern side in Nova Icaria and Somorrostro (P_3).

At all beaches the temporal (Fig. 6b) and spatial (Fig. 6d) eigenfunctions of the second mode of the EOFs show a series of oscillations that occur at a faster temporal scale (ranging from weeks to months), roughly responding to storm events. The second spatial eigenfunction describes the shoreline translation but also contains information on beach planform rotation ($E_2(x)$ crosses zero while for the case of translation it should be a horizontal line, see Fig. 6). Rotation movements are predominant in profile P_3 – P_5 while translation movements are in P_6 – P_{10} .

The sign of the second combined eigenfunction is negative in August 2005 and 2006 when stormy events (following accretional periods) occurred. According to the observations reported (Yates et al.,

Table 3

Percentage of the total variability G_k (percent variance explained) represented by the first three eigenfunctions at Barcelona beaches.

Data set	G_1	G_2	Remaining
Bogatell	70.2%	27%	0.8%
Nova Icaria	78.08%	20%	1.92%
Somorrostro	80.73%	18%	1.27%

2009), a storm (not necessarily a major one) following an accretional period is likely to cause more erosion than the same storm over an already eroded beach. This process is happening also in this case of study and properly captured by the eigenfunction analysis as shown in Fig. 5a where shoreline retreat is clearly observed after high energy conditions produced in August 2005 and August 2006 (blue colour).

With respect to the interpretation of the second eigenfunction, the spatial component displays, for all beaches, smaller variations from P_1 to P_{10} (variations in $E_1(x)$) are approximately twice as large as the variations in $E_2(x)$). Also, the second temporal eigenfunction, $C_2(t)$, displays changes occurring at a temporal scale that is faster than the changes observed in $C_1(t)$. Summarizing, more rapid (in time) and smaller (in space) changes are associated to the second eigenfunction (the opposite can be said about the first eigenfunction) which we have interpreted as the result of short duration storms.

The combined eigenfunction $E_2(x) \cdot C_2(t)$ shows alternating cycles of beach movement (Fig. 8). Such changes represent a combination between translation and rotation movements and they appear to be larger at the north end of each beach probably because that is the

area that is affected by the presence of the breakwater under varying directions of wave approach.

The remaining combined eigenfunctions account for only slightly less than 3% of the total variability, therefore a detailed analysis is not warranted.

The total shoreline change, measured from video images, was described by two components: translation and rotation. Shoreline rotation is shown in Fig. 6a which displays evident rotation patterns occurring approximately simultaneously at the 3 beaches. Some of the rotation events are not uniform but, especially at Bogatell (the longest of the beaches analysed), are involved by single storm events which temporarily affect the overall rotation pattern.

5.2. Wave characteristics and shoreline movement

The total shoreline change, measured from video images, was described by two components: rotation TM_{rot} and translation $TM_{tr,\pi}$.

The shoreline rotation evaluated at profiles P_{10} and P_1 of each beach of Barcelona is shown in Fig. 9a and b. Shoreline rotation at P_{10} oscillates and changes from negative to positive signs between winter (From November to April) and summer (from May to October) months. Positive and negative oscillations are observed in winter and summer at P_1 , respectively. Local changes in shoreline rotation are associated to high frequency oscillations with a period of days to months.

Shoreline rotation at all profiles of studied beaches is presented in Fig. 5b which is consistent with the first EOF combined eigenfunction (Fig. 7). We can notice that, at all beaches analysed, rotation occurs slowly with the overall beach planform becoming more uniform (see for

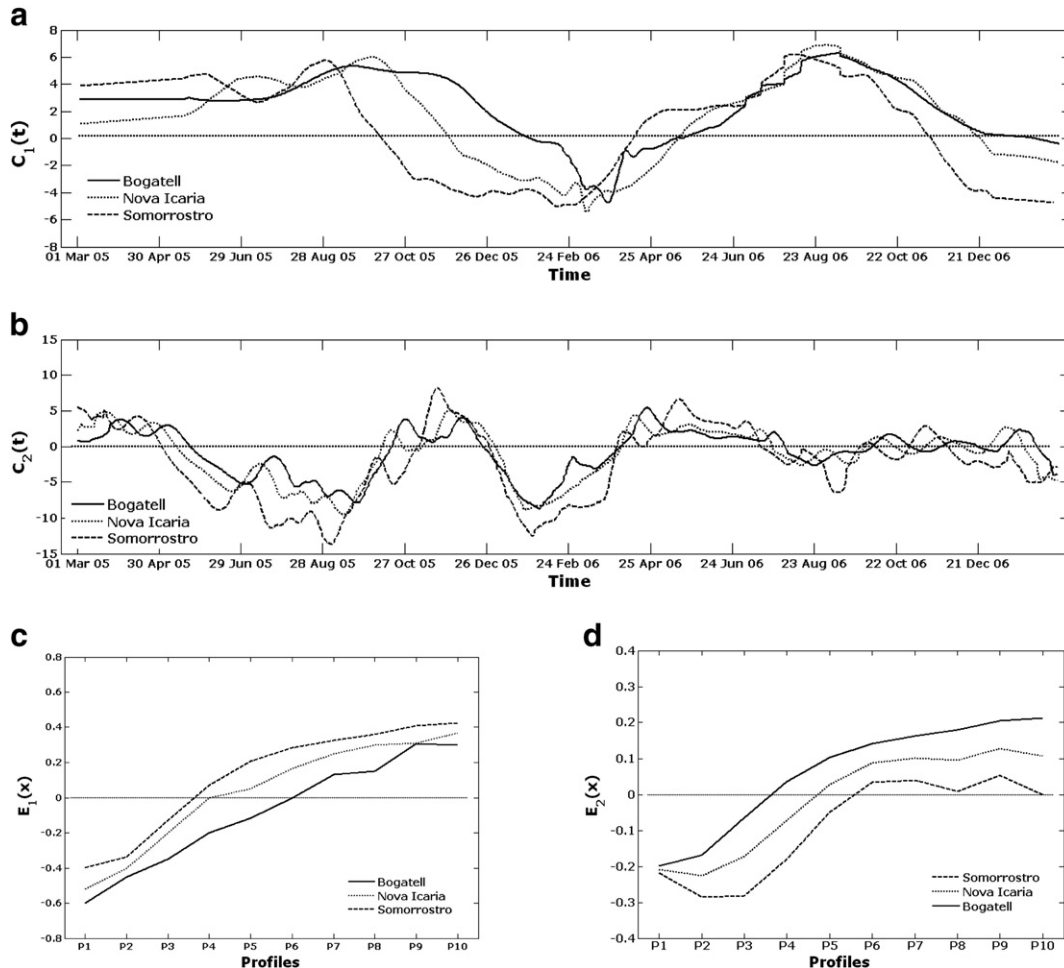


Fig. 6. First (a) and second (b) temporal eigenfunctions based on a EOF analysis of the beach change in Barcelona beaches. First (c) and second (d) spatial eigenfunctions based on a EOF analysis of beach change in Barcelona beaches. Bogatell (solid line), Nova Icaria (dotted line) and Somorrostro (dashed line).

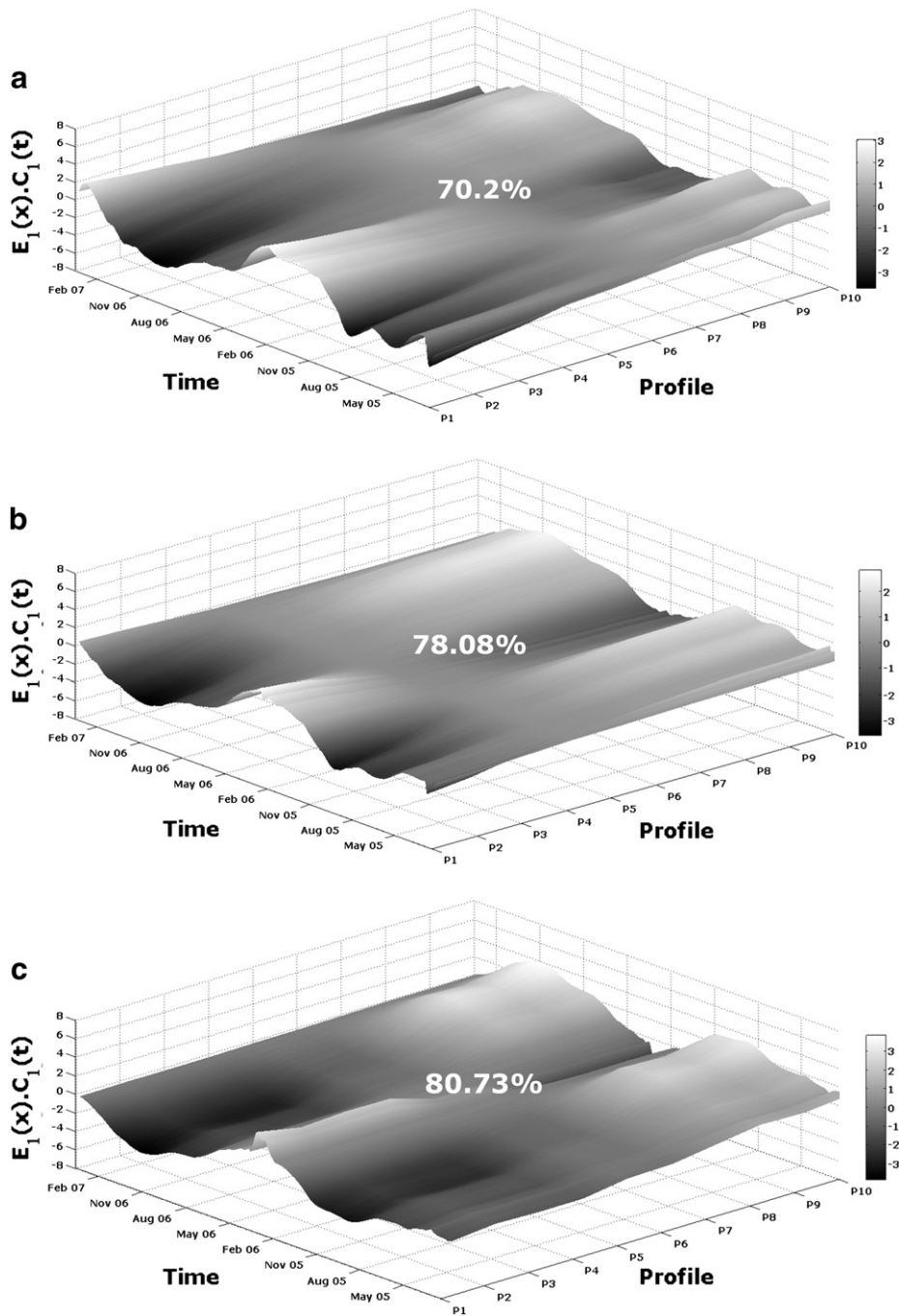


Fig. 7. First combined eigenfunction ($Y_1(x,t) = C_1(t). E_1(x)$). (a) Bogatell, (b) Nova Icaria, and (c) Somorrostro.

example the period around the end of October 2005). Following this period, there is usually a major storm (like the one occurring at the beginning of November 2005) or a sequence of storms that causes beach rotation. This sequence of morphological changes (initial smoothing followed by a rotation) can be observed for the other beach rotation events (Fig. 5b). At the same time, the more detailed wave analysis shown in Fig. 2b where wave rose indicates distinct changes between winter and summer in terms of both wave height and wave direction.

Shoreline translation, presented in Fig. 9c shows patterns of cross-shore variations characterized by a series of low frequency (order of months) oscillations corresponding to shoreline advance in summer time and retreat due to energetic conditions during winter months

(from October to April). At the shorter-scale, there are equally large oscillations with negative trends produced over high stormy events such as the one that occurred on 31-Dec-2005 and 26-Jan-2006.

A comparison of Figs. 6 and 9 shows that the EOF and calculated patterns of rotation and translation are consistent after February 20th. With respect to beach rotation (herein considered to be represented by the first EOF mode) the differences between the two methods only relate to the smaller level of fast-scale statistical fluctuations present in the EOF analysis. In essence the first mode of the EOF analysis primarily captures the very broad coherent beach behaviour. Results provided by EOFs and the conceptual method are not similar before February 20th when a description of the shoreline rotation

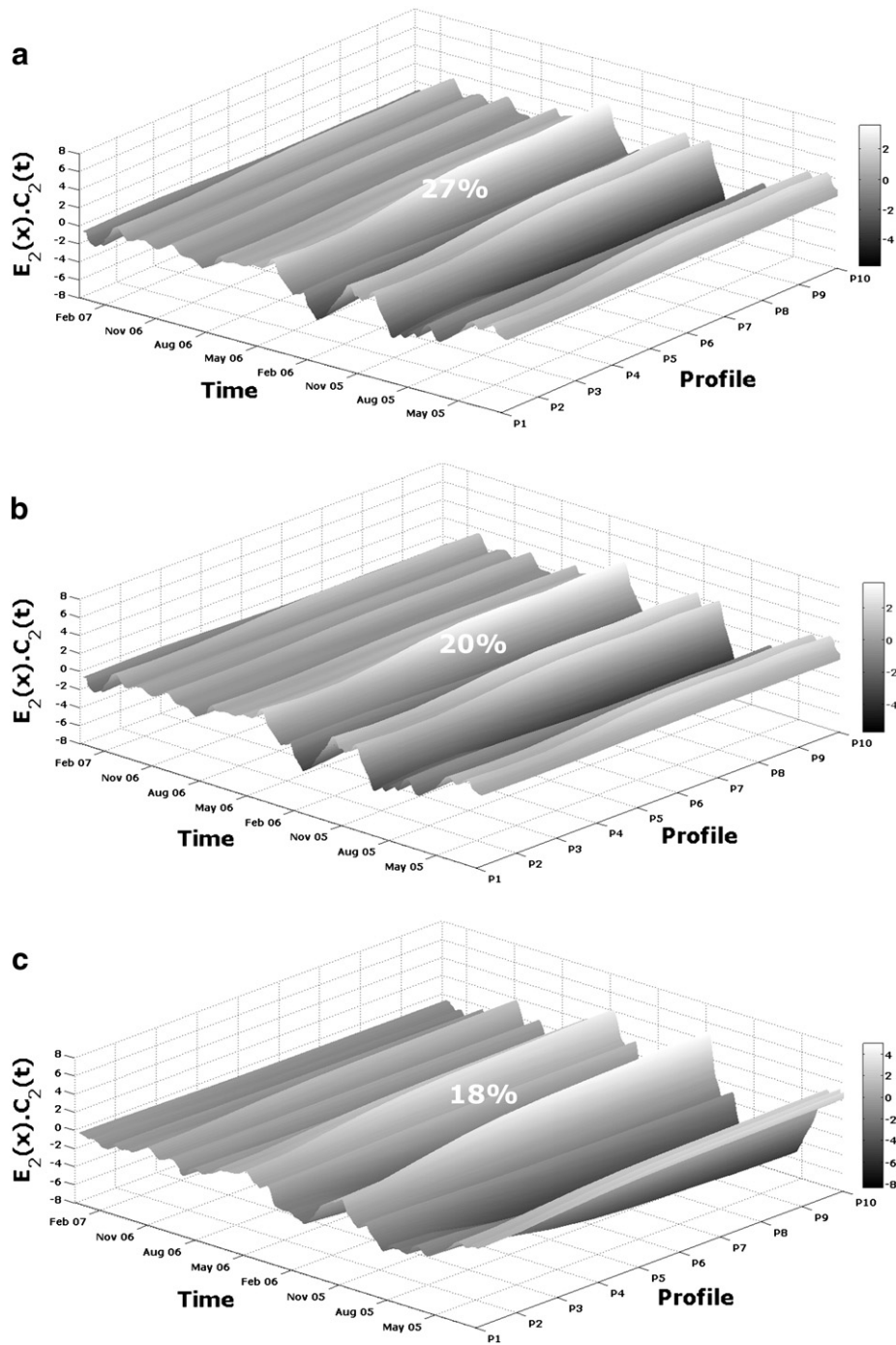


Fig. 8. Second combined eigenfunction ($Y_2(x,t) = C_2(t) \cdot E_2(x)$). (a) Bogatell, (b) Nova Icaria, and (c) Somorrostro.

requires using both EOF modes (some information of shoreline rotation is clearly part of the second mode). The discrepancy between the first EOF mode and the measured rotation is particularly evident for Bogatell where in fact the E_2 of profile P_{10} is larger compared to the other beaches.

Shoreline movement, at a time t_j , is defined as a response of the beach to individual observations of energy conditions which are integrated over the k th preceding days t_{j-k} in order to put emphasis the influence of the antecedent wave conditions in the shoreline response of t_j . This relation was explored in this research to put emphasis the influence of the antecedent wave conditions in the shoreline response

of t_j . Translation and rotation movement were correlated to the averaged EF_{csh} and EF_D , respectively. EF_{csh} was averaged between 1 and 20 preceding days while EF_D was averaged between 1 and 55 days. The translation component is the same for all profiles at each beach while for the rotation we considered the values estimated for profiles P_{10} and P_1 at each of the beach studied.

Fig. 10 shows the goodness of fit between EF_{csh} and translation TM_{tr} , and between EF_D and rotation TM_{rot} . Significant ($p < 0.05$) correlation coefficients, R^2 , between the averaged EF_{csh} and the shoreline translation were found for EF_{csh} averaging between 5 and 9 preceding days at Somorrostro, between 7 and 12 preceding days at Nova Icaria

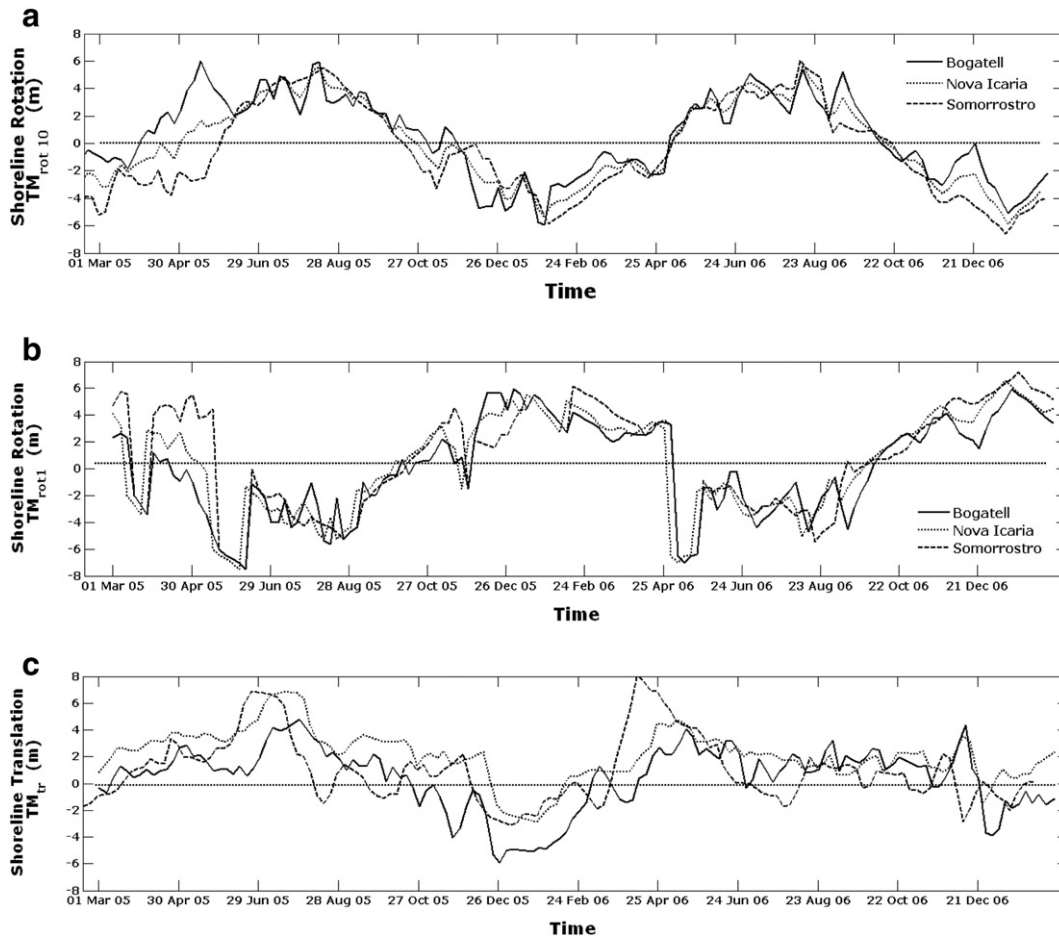


Fig. 9. Analysis of the shoreline rotation TM_{rot10} (a), TM_{rot1} (b) and the shoreline translation TM_{tr} (c) at Barcelona beaches.

and between 9 and 14 at Bogatell. Maximum R^2 were detected for EF_{csh} averaging 7, 10 and 11 days at Somorrostro, Nova Icaria and Bogatell, respectively (Fig. 10a).

The averaged EF_D and the shoreline rotation were significantly correlated ($p < 0.05$) averaging between 25 and 35 preceding days at Somorrostro, between 30 and 40 days at Nova Icaria and 32 and 43 days at Bogatell. Highest R^2 was observed for an averaged EF_D of 28, 34 and 40 days at Somorrostro, Nova Icaria and Bogatell, respectively (Fig. 10b).

The temporal evolution between the rotation, at profiles P_{10} and P_1 , and the 28 day-averaged EF_D , and between the translation and the 7 day-averaged EF_{csh} at Somorrostro is presented in Fig. 11.

Clockwise and counter-clockwise rotations of Somorrostro beach are related to positive and negative changes of the shoreline at the profile P_{10} (Fig. 11a). The first case can be produced under a predominance of the south–south–east wave direction. While, predominance of east–south–east waves implies negative changes in beach orientation. An opposite scenario is observed for P_1 as seen in Fig. 11b where clockwise rotations are explained by waves coming from east–south–east. Similar results are obtained for Nova Icaria and Bogatell.

As seen in Fig. 11c, large values of the averaged EF_{csh} are related to large changes of shoreline translation implying changes in the beach profile. Low values of the averaged EF_{csh} and concomitant large values of EF_D imply predominance of alongshore sediment transport and are therefore associated to beach rotation.

6. Discussion and conclusions

A video system was used to monitor and study three artificial pocket beaches along the Barcelona city coast. These beaches experience the

same offshore wave conditions but differ in their geomorphic characteristics. Nova Icaria and Bogatell have the same sediment grain size (0.75 mm) but different length (600 m and 400 m respectively). In contrast, Nova Icaria and Somorrostro have the same length but Somorrostro is characterized by a finer grain size (0.45 mm).

The method for extracting the shoreline position from time-averaged video images has been shown to be accurate when compared to DGCP data. The ability to capture shoreline changes at a high temporal and spatial resolution provides an ideal dataset to study shoreline variations.

An EOF analysis was used to decompose the demeaned dataset of shoreline positions into the constituent modes of change. The first mode of variability is related to shoreline plan-form rotation which occurs at the seasonal temporal scale. The second mode is related to the cross-shore shoreline translation which occurs at a faster scale (order of weeks).

These observations are in contrast with the study of Harley et al. (2012) at Collaroy–Narrabeen where the dominant mode is the storm-driven onshore–offshore movement. The reason for the difference can be attributed to the different (1) climatic conditions which are more energetic at Collaroy–Narrabeen (average $H_s = 1.6$ m) than at Barcelona (average $H_s = 0.7$ m); (2) beach sediments which are finer at Collaroy–Narrabeen ($D_{50} = 0.3$ mm) than at Barcelona beaches (D_{50} more than 0.4 mm) implying faster response of the beach profile which is mainly controlled by the sediment grain size; (3) beach length (3.6 km at Collaroy–Narrabeen) which is more than 6 times larger than at Barcelona beaches considered in this study (around 600 m) which implies that the plan-form rotation, involving larger amounts of sand, is slower and less frequent than this observed at small beaches.

Two of the beaches studied in this work, Bogatell and Nova Icaria, although for a different period of time (2001–2005), were also investigated

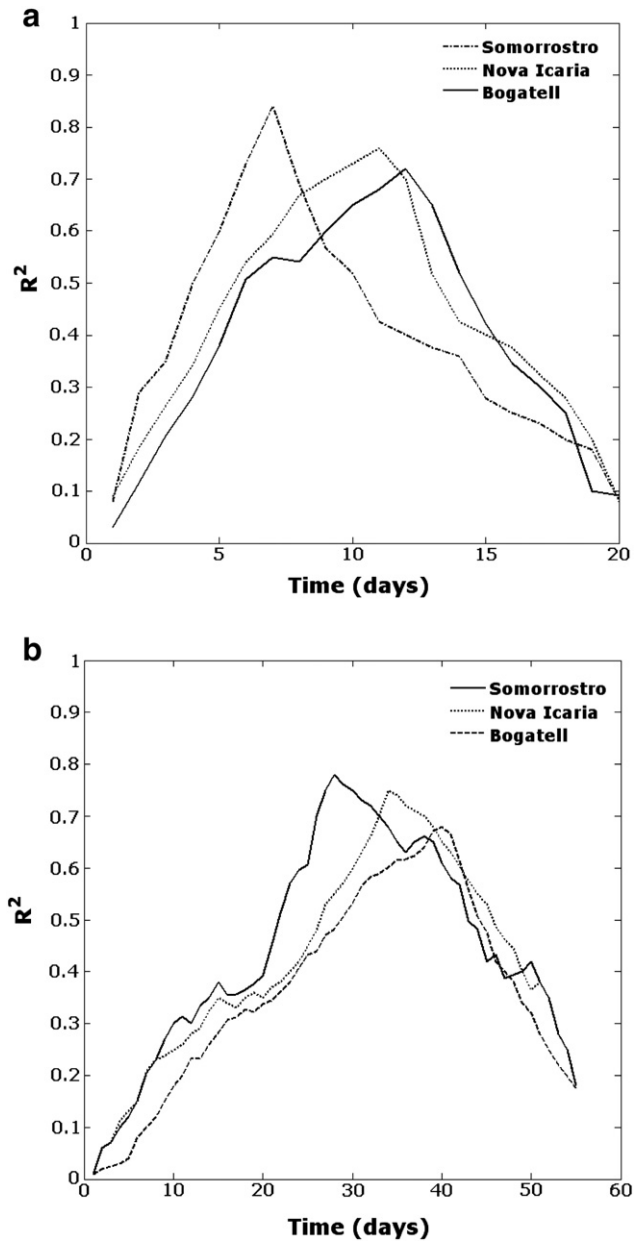


Fig. 10. Goodness-of-fit, R^2 , of the correlation between (a) shoreline translation TM_{tr} and the time-averaged EF_{csh} and (b) shoreline rotation TM_{rot10} (at P_{10}) and the time-averaged EF_D . The grey horizontal line represents the $p = 0.05$ level of significance.

by Ojeda and Guillén (2008) using video data to assess the main factors affecting shoreline dynamics. The study related shoreline rotation to beach nourishment (notice that during our study-period no nourishment was performed) and gradual recovery of the beach after stormy periods. Episodes of beach rotation occurring during storms were related to the alongshore component of the radiation stress, a parameter consistent with the energy flux direction (EF_D) used in this study.

For all modes of change, extracted from EOF analysis, the response of the shoreline to wave energy is dictated by the physical characteristics of the beaches such as sediment grain size and beach length. The response is in fact faster at Somorrostro, which is characterized by finer sediment material, than at Nova Icaria one. It is even slower at Bogatell where the beach length is larger.

The EOF results provide a general statistical analysis and the principal components governing the shoreline variability. Still, EOF does not necessarily separate translation from rotation and some of the signal.

The total shoreline variability observed at Barcelona beaches is a combination of the plan-form rotation and the profile translation produced in the cross-shore direction. The conceptual model proposed to separate translation and rotation movement of the beach implies a series of simplifications. In particular, we assume a linear planform shape of the beach and a constant beach profile. Also, if beach rotation is defined as the lateral movement of sand towards alternating ends of an embayed beach (Short and Masselink, 1999), there is the possibility that differential cross-shore shoreline movements, or any other perturbation to a uniform cross-shore translation, are considered as rotation events. This could result in an overestimation of beach rotation. The assumption that advances and retreats are driven by a longshore current rather than gradients in wave height is justified by numerical modelling (not shown) indicating that alongshore variations in wave height immediately prior to breaking are small at all beaches. Only for waves approaching from the east, the shortest beaches (Somorrostro and Nova Icaria) could be affected by along-shore gradients in wave heights. Aside from this case alongshore gradients are minimal.

The process of beach rotation is a fast response of recovery to high energy conditions produced at short-scales and man-made changes in the beach orientation resulting from nourishment or sand relocation as stated by (Ojeda and Guillén, 2008). In this research, we studied, for a period where no man-made changes occurred, not only the short-term (storms) changes in beach rotation but also the medium-term (seasonal scale) changes showing that changes in oblique wave incidence and energy conditions from winter to summer can be responsible for beach rotation around a pivotal zone.

Rotation and translation were statistically correlated to the previous wave conditions. Time-averages of cross-shore radiation stress EF_{csh} and of energy flux direction EF_D resulted in statistically significant correlations with shoreline translation and rotation (at the profile P_{10}) for all beaches (Fig. 10a and b).

Shoreline rotation and translation at Bogatell, the longest beach, were correlated to the 40-day-averaged EF_D and the 12-day-averaged EF_{csh} . The number of days at which the correlation is highest decreases at Nova Icaria (same sediment grain size but shorter beach length than Bogatell) and decreases even more at Somorrostro (smaller grain size and shorter beach length). Therefore, the shoreline rotation depends on the sediment grain size D_{50} and the beach length l in such a way that larger beach lengths and finer sediments result in a faster response of its plan-form to wave action. In contrast, the translation movement of the shoreline is supposed to be only controlled by the sediment grain size D_{50} . In fact, the number of days maximising the correlation between TM_{tr} and the averaged EF_{csh} is 7 days in Somorrostro (fine sediments 0.45 mm) and increases to 11 and 12 days in Nova Icaria and Bogatell beaches (same sediments size 0.75 mm). Differences between Nova Icaria and Bogatell (Fig. 10a) can be attributed to either differences in the details of the granulometric curves or, more likely, are an indication that our simplified separation between rotation and translation does not fully capture the nature of observed beach changes.

Overall, our finding indicates that the timescales for shoreline rotation and translation are different and that the shoreline response is strongly controlled by the physical characteristics of each beach. Rotation is the dominant mode of variability and its response to previous forcing conditions is such that the greater the length of the beach and its sediment grain size, the slower its response.

Acknowledgement

This work has been conducted as part of PhD which is funded by the Spanish Ministry of Science and Technology within the project “Modelado de la Evolución Morfodinámica de Playas en Medio Plazo” (CTM2008-06640). Thanks to the Coastal Ocean Observatory at ICM (CSIC) in Barcelona (Spain) and in particular Jorge Guillén for providing video images.

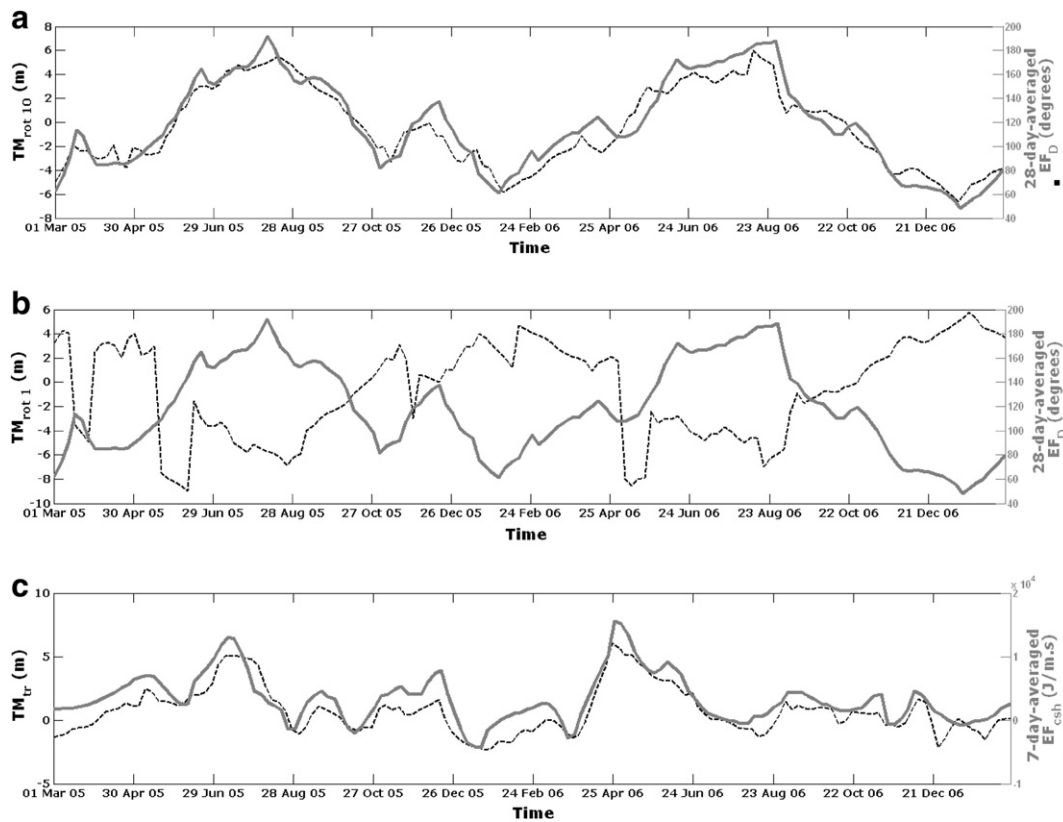


Fig. 11. Best correlation between the standardized 28 day-averaged EF_D and the shoreline rotation at P_{10} (a) and P_1 (b). (c) Correlation between the standardized 7 day-averaged EF_{csh} and the shoreline translation.

References

- Aarninkhof, S.G.J., Caljouw, M., Stive, M.J.F., 2000. Video-based, Quantitative Assessment of Intertidal Beach Variability. : Proceeding of 27th International Conference of Coastal Engineering, 4. ASCE, pp. 3291–3304.
- Aarninkhof, S.G.J., Turner, I.L., Dronkers, T.D.T., Caljouw, M., Nipius, L., 2003. A video-based technique for mapping intertidal beach bathymetry. *Coastal Engineering* 49, 275–289.
- Aubrey, D., 1979. Seasonal patterns of onshore/offshore sediment movement. *Journal of Geophysical Research* 84 (C10), 6347–6354.
- Bryan, K.R., Gallop, S.L., Van-de-Lageweg, W.I., Coco, G., 2009. Observations of rip channels, sandbar-shoreline coupling and beach rotation at Tairua Beach, New Zealand. Proceeding of 19th Australasian Coastal and Ocean Engineering Conference, Coasts and Ports, pp. 1–6.
- Davidson, M., Knoningsveld, M.V., Holman, R.A.K.A., Medina, R., Aarninkhof, S.J.G., 2007. The coastview project: developing video-derived coastal state indicators in support of coastal zone management. *Coastal Engineering* 54, 463–476.
- Davidson, M., Lewis, P.R., Turner, I.L., 2010. Forecasting seasonal to multi-year shoreline change. *Coastal Engineering* 57, 953–958.
- Davidson, M., Turner, I.L., Guza, R.T., 2011. The effect of temporal wave averaging on the performance of an empirical shoreline evolution model. *Coastal Engineering* 58, 802–805.
- Fairely, I., Davidson, M., Kingston, K., Dolphin, T., Phillips, R., 2009. Empirical orthogonal function analysis of shoreline changes behind two different designs of detached breakwaters. *Coastal Engineering* 29 (1), 59–76.
- Farris, A.S., List, J.H., 2007. Shoreline change as a proxy for subaerial beach volume. *Journal of Coastal Research* 23, 740–748.
- Frasier, S.J., Liu, Y., Moller, D., McIntosh, R.E., Long, C., 1995. Directional ocean wave measurements in a coastal setting using focused array imaging radar. *IEEE Transactions on Geoscience and Remote Sensing* 33.
- Gonzalez, M., Medina, R., 2007. An integrated coastal modeling system for analyzing beach processes and beach restoration projects, SMC. *Computers & Geosciences* 33.
- Gonzalez, M., Medina, R., Losada, M., 2010. On the design of beach nourishment projects using static equilibrium concepts: application to the Spanish coast. *Coastal Engineering* 57, 227–240.
- Guedes, R., Bryan, K., Coco, G., Holman, R., 2011. The effects of tides on swash statistics on an intermediate beach. *Journal of Geophysical Research* 116, C04008.
- Harley, M.D., Turner, I.L., Short, A.D., Ranasinghe, R., 2010. Interannual variability and controls of the Sydney wave climate. *International Journal of Climatology* 30, 1322–1335.
- Harley, M.D., Turner, I.L., Short, A.D., Ranasinghe, R., 2012. A re-evaluation of coastal embayment rotation: the dominance of cross-shore versus alongshore sediment transport processes, Collaroy–Narrabeen, beach, Australia. *Journal of Geophysical Research* 116, F04033. <http://dx.doi.org/10.1029/2011JF001989>.
- Holland, R.A., Stanley, J., 2007. The history and technical capabilities of Argus. *Coastal Engineering* 54, 477–491.
- Holland, K.T., Holman, R.A., Lippman, T.C., Stanley, J., Plant, N., 1997. Practical use of video imagery in nearshore oceanographic studies. *IEEE Journal of Oceanic Engineering* 22 (1), 135–150.
- Holman, R.A., Lippmann, T.C., 1987. Remote sensing of nearshore bar systems: making morphology visible. In: N. Y. American Society of Civil Engineering (Ed.), *Conference Coastal Sediments '87*, New Orleans.
- Holman, R.A., Symonds, G., Thornton, E.B., Ranasinghe, R., 2006. Rip spacing and persistence on an embayed beach. *Journal of Geophysical Research* 111, C01006. <http://dx.doi.org/10.1029/2005JC002965>.
- Klein, A.H.F., Filho, A.B., Shumacher, D.H., 2002. Short-term beach rotation processes in distinct headland bay beach systems. *Journal of Coastal Research* 18, 442–458.
- Larson, M., Jansen, M., Rozynski, H., Southgate, H.N., 2003. Analysis and modelling of field data on coastal morphological evolution over yearly and decadal time scales. Part 1: background and linear techniques. *Journal of Coastal Research* 19 (4), 760–775.
- Martins, C., de Mahiques, M., Dias, J.M.A., 2010. Evolution of longshore beach contour lines determined by the EOF method. *Earth Surface Processes and Landforms* 35, 487–495.
- Masselink, G., Pattiaratchi, C.B., 2001. Seasonal changes in beach morphology along the sheltered coastline of Perth Western Australia. *Marine Geology* 172, 243–263.
- Medina, R., Vidal, C., Losada, M.A., Roldan, R.J., 1991. Three-mode principal component analysis of bathymetric data, applied to 'Playa de Castilla'. Proceedings of 23rd International Conference on Coastal Engineering, ASCE, New York, pp. 2265–2278.
- Medina, R., Losada, M.A., Losada, I.J., Vidal, C., 1994. Temporal and spatial relationship between sediment grain size and beach profile. *Marine Geology* 118, 195–206.
- Miller, J.K., Dean, R., 2007a. Shoreline variability via empirical orthogonal function analysis: part I: temporal and spatial characteristics. *Coastal Engineering* 54, 111–131.
- Miller, J.K., Dean, R., 2007b. Shoreline variability via empirical orthogonal function analysis: part II: relationship to nearshore conditions. *Coastal Engineering* 54, 133–150.
- Ojeda, E., Guillén, J., 2008. Shoreline dynamics and beach rotation of artificial embayed beaches. *Marine Geology* 253, 51–62.
- Ojeda, E., Guillén, J., Ribas, F., 2010. The morphodynamic responses of artificial embayed beaches to storm events. *Advances in Geosciences* 6, 99–103.
- Ojeda, E., Guillén, J., Ribas, F., 2011. Dynamics of single-barred embayed beaches. *Marine Geology* 280, 76–90.
- Osorio, A., Desarrollo de cámaras de vídeo para hacer seguimiento de las actividades de dragado en los canales de navegación. Ph.D. thesis, Universidad de Cantabria, Santander, Spain, 2006.
- Ranasinghe, R., McLoughlin, R., Short, A., Symonds, G., 2004. The southern oscillation index, wave climate and beach rotation. *Marine Geology* 204, 273–287.

- Robertson, V.W., Whitman, D., Zhang, K., Leatherman, S.P., 2004. Computer simulation models of a hooked beach shoreline configuration. *Journal of Coastal Research* 20, 884–892.
- Ruiz-De-Alegria-Arzaburu, A., Masselink, G., 2010. Storm response and beach rotation on a gravel beach, Slapton Sands, UK. *Marine Geology* 57.
- Short, A.D., Masselink, G., 1999. Beach and shoreface morphodynamics. Chap. Embayed and Structurally Controlled Beaches, pp. 230–250 (Chichester).
- Short, A.D., Cowell, P.J., Cadee, W., Hall, W., Dijk, B.V., 1995. Beach rotation and possible relation to southern oscillation. *Ocean Atmosphere Pacific Conference*, pp. 329–334.
- Short, A.D., Trembanis, A.C., Turner, I.L., 2000. Beach oscillation, rotation and the southern oscillation, Narraben Beach, Australia. *Proceeding of the 27th International Conference on Coastal Engineering, Australia*, pp. 2439–2456.
- Smith, R.K., Bryan, K.R., 2007. Monitoring beach face volume with a combination of intermittent profiling and video imagery. *Journal of Coastal Research* 23, 892–898.
- Stockdon, H.F., Holman, R.A., 2000. Estimation of wave phase speed and nearshore bathymetry from video imagery. *Journal of Geophysical Research* C9 (105), 22,015–22,033.
- van Enckevort, I., Ruessink, B., Coco, G., Suzuki, K., Turner, I.L., Plant, N., Holman, R., 2004. Observations of nearshore crescentic sandbars. *Journal of Geophysical Research* 109 (1), C06028. <http://dx.doi.org/10.1029/2003JC002,214>.
- von Storch, H., Hannstock, G., 1984. Comment on “empirical orthogonal function analysis of wind vectors over the tropical pacific region”. *Bulletin of the American Meteorological Society* 65, 1621.
- Winant, C.D., Inman, D.L., Nordstron, C.E., 1975. Description of seasonal beach changes using empirical eigenfunctions. *Journal of Geophysical Research* 80 (15), 1979–1986.
- Yates, M.L., Guza, R.T., Reilly, W.C.O., 2009. Equilibrium shoreline response: observations and modelling. *Journal of Geophysical Research* 114. <http://dx.doi.org/10.1029/2009JC005359>.